Vibrational Spectrum of Katoite $Ca_3Al_2[(OH)_4]_3$: A Periodic ab Initio Study

R. Orlando,[†] F. J. Torres,[‡] F. Pascale,[§] P. Ugliengo,[||] C. Zicovich-Wilson,[⊥] and R. Dovesi*[,||]

Dipartimento di Scienze e Tecnologie Avanzate, Università del Piemonte Orientale, Via Bellini 25/G, 15100 Alessandria, Italy, Dipartimento di Chimica IFM, Università di Torino, Via P. Giuria 7, 10125 Torino, Italy, Laboratoire de Cristallographie et Modélisation des Matériaux Minéraux et Biologiques, UMR-CNRS-7036, Université Henri Poincaré−Nancy I, B.P. 239, 54506 Vandoeuvre-lès-Nancy Cedex 05, France, Dipartimento di Chimica IFM, Università di Torino and Nanostructured Interfaces and Surfaces (NIS) Centre of Excellence, http://www.nis.unito.it, Via P. Giuria 7, 10125 Torino, Italy, and Universidad Autónoma del Estado de Morelos, Av. Universidad, 1001, Col. Chamilpa, 62210 Cuernavaca (Morelos), México

Received: July 1, 2005; In Final Form: November 15, 2005

The vibrational spectrum of the Si-free katoite hydrogarnet (116 atoms in the unit cell) has been calculated at the periodic ab initio quantum mechanical level with the CRYSTAL program, by using a Gaussian type basis set and the hybrid B3LYP Hamiltonian. The harmonic frequencies at the Γ point have been obtained by diagonalizing the mass-weighted Hessian matrix, that is evaluated by numerical differentiation of the analytical first derivatives of the energy with respect to the atomic Cartesian coordinates. The parameters controlling the numerical differentiation, as well as the numerical integration of the exchange-correlation functional for the self-consistent field (SCF) calculation, are shown to affect the obtained frequencies by less than 3 cm^{-1}. Before diagonalization, the dynamical matrix is transformed to a block diagonal form according to the irreducible representations of the point group, so that the 345 vibrational modes are automatically classified by symmetry. Various tools are adopted (graphical representation, isotopic substitution, "freezing" part of the unit cell) that permit a complete classification of normal modes and, in particular, an analysis of the modes in terms of simple models (octahedra modes, Ca modes, H stretching, bending, rotations). The harmonic OH stretching band (48 modes) is quite narrow (20 cm^{-1}), indicating that the interaction among OH groups is very weak. As the OH stretching modes are known to be totally separable from the other modes and strongly anharmonic, the one-dimensional Schroedinger equation for the anharmonic oscillator is solved numerically for the two extreme situations, corresponding to the vibration of one decoupled OH and of all 48 OH groups moving in phase. The anharmonic frequencies are 3682 and 3673 cm^{-1}, respectively, in good agreement with IR experiments (a single band at 3661 cm^{-1} with a width at half band height of 33 cm^{-1}) and confirming that the interaction between OH groups is extremely weak.

I. Introduction

The problem of incorporating hydrogen in nominally anhydrous minerals has great relevance from both a technological and a speculative point of view, and it has been discussed in the literature in the last 35 years.[1−5] Due to their stability, chemical variability, and abundance in the earth mantle, garnets are among the most interesting possible hydrogen *reservoirs*. Starting from grossular $Ca_3Al_2(SiO_4)_3$, it is possible to substitute $(OH)_4$ groups for all of the SiO_4 groups (each H being bonded to one of the O atoms formerly linked to silicon) and the resulting compound, $Ca_3Al_2(O_4H_4)_3$, is usually called katoite or hydrogrossular. Other members of the solid solution series between the two end-members, where the Si substitution is only partial, have been characterized from many points of view,[6−8] and they are stable structures.

In a previous paper,[9] the equilibrium geometry at room pressure, the formation energy, the equation of state, and the effect of pressure on the geometry of the $(OH)_4$ "defect" have been investigated with the CRYSTAL code, using a Gaussian basis set and the B3LYP functional. The computed results are in excellent agreement with experiment.[10−12] For example, calculated and experimental[13,14] formation enthalpies for grossular and katoite from simple oxides and water are (in kilojoules per mole) −320 and −245 to be compared with −330 and −256 ± 12, respectively.

In regard to vibrational properties, the OH total-symmetric mode (all 48 OH groups moving in phase) was investigated by solving numerically the one-dimensional Schroedinger equation corresponding to the anharmonic oscillator whose potential energy surface has been obtained by performing a set of total energy calculations at various OH distances.[9] The computed totally symmetric B3LYP anharmonic ω_{01}(OH) frequency at 3670 cm^{-1} is in remarkable agreement with the experimental result of Rossman and Aines[4] (see sample number 1059, $x = 0$), who recorded a single IR band at 3663 cm^{-1}, with a width at half band height (WHBH) of about 35 cm^{-1} and with the recent IR spectra obtained by Kolesov and Geiger[38] who

* Corresponding author. E-mail: roberto.dovesi@unito.it.
[†] Università del Piemonte Orientale.
[‡] Università di Torino.
[§] Université Henri Poincaré−Nancy I.
[||] Università di Torino and Nanostructured Interfaces and Surfaces (NIS) Centre of Excellence.
[⊥] Universidad Autónoma del Estado de Morelos.

10.1021/jp053602j CCC: $33.50
Published on Web 12/22/2005

reported a value of 3661 and a WHBH of 33 cm^{-1}. The presence of a single peak in the experimental spectrum suggests that the interaction within the $(OH)_4$ defect and among the 12 $(OH)_4$ groups in the unit cell is quite weak at room pressure.

Recently, tools have been implemented in the CRYSTAL code that permit extension of the previous study[9] to the full harmonic vibrational spectrum of katoite at Γ.[15,16] The influences of the computational parameters, basis set, and selected Hamiltonian on the calculated frequencies have been discussed in refs 15 and 16 with reference to α-quartz, where the accuracy of the proposed method has been documented. Among other features, the method permits automatic symmetry classification of the modes, with great simplification of the present analysis, where 345 modes belong to 10 irreducible representations. The present system is however peculiar for the presence of 48 OH groups, with anharmonic effects that can be as large as 150−200 cm^{-1} for the OH stretching. It has been shown in two recent papers[17,18] that (i) it is possible to take anharmonicity effects into account at a quantum mechanical level and (ii) B3LYP provides accurate OH stretching frequencies, whereas LDA and PBE do not perform equally well.[18,19] This new set of computational tools is now applied to a complete analysis of the harmonic vibrational features of katoite at Γ and for the complementary investigation of anharmonicity effects in the OH stretching.

The interpretation of the main features of a spectrum, such as the origin of low frequency modes and the participation of atoms or chemical groups in the various modes, in terms of simple models, is one of the crucial points for the investigation of large unit cell systems, with hundreds of modes. It will be shown in the following that quantitative or semiquantitative answers to most of these issues are at hand.

Katoite has a cubic structure with the $Ia\bar{3}d$ space group, the same as grossular $Ca_3Al_2Si_3O_{12}$, from which it can be derived. In grossular, SiO_4 tetrahedra share corners with AlO_6 octahedra to form a strongly connected network of covalent (or semicovalent) bonds. The network of tetrahedra and octahedra delimit triangular dodecahedra containing Ca cations that form fully ionic bonds with oxygen. The covalent net of grossular is broken in katoite at the tetrahedra site level, where four H atoms, each one bonded to its nearest oxygen neighbor, are substituted for one Si atom connecting four different O atoms, as shown in Figure 1. The modification of the covalent skeleton has a strong influence on elastic properties (the bulk modulus of katoite is between 52 and 66 GPa,[10,20,21] whereas typical values for garnets, such as pyrope and grossular, are within 165 and 180 GPa)[22,23] and vibrational features, as will be discussed in the next section.

II. Computational Methods

For the present calculations, a development version of the CRYSTAL program has been used.[24] CRYSTAL is a periodic ab initio program that uses a Gaussian type basis set. In the present case, all-electron basis sets[25] have been adopted, with 8-6511G(d), 8-511G(d), 8-411G(d), and 31G(p) contractions for Ca, Al, O, and H, respectively (8-6511G(d) means that the first shell, of s type, is a contraction of eight Gaussians; four sp contractions containing six, five, one, and one Gaussians follow; a 5d shell completes the Ca basis). The exponent (in $bohr^{-2}$ units) of the most diffuse sp shell has been reoptimized for the present system and is 0.28 (Ca), 0.28 (Al), 0.22 (O), and 0.16 (H).

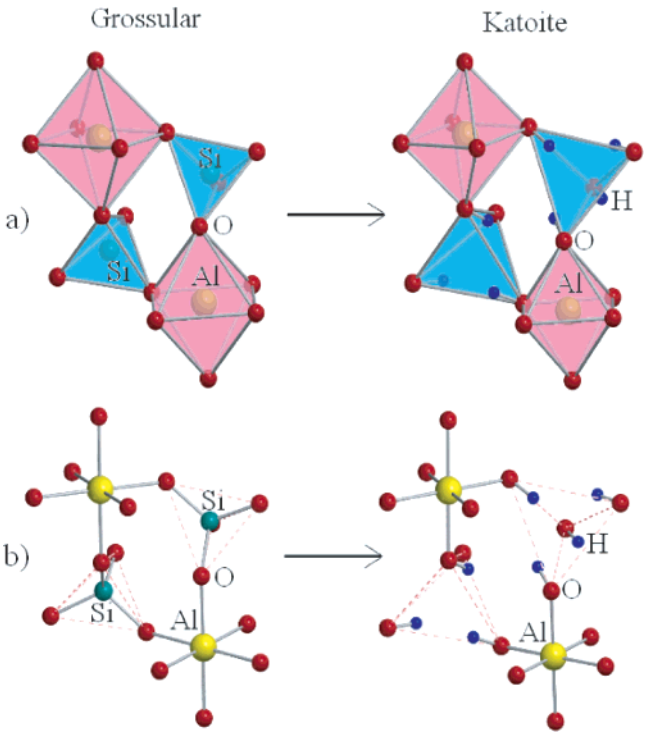

Figure 1. Loss of covalent connectivity in the transformation of grossular into katoite. Only part of the unit cell is shown, containing two AlO_6 octahedra and two SiO_4 tetrahedra or $(OH)_4$ defects. Calcium dodecahedra are not shown: (a) polyhedra representation; (b) representation of covalent and semicovalent bonds.

The B3LYP Hamiltonian[26] has been used, which contains a hybrid Hartree−Fock/density-functional exchange-correlation term. Such a Hamiltonian is used widely and successfully in molecular quantum chemistry,[27] as well as in solid state calculations, where it has been shown to provide excellent results for geometries and vibration frequencies,[16,28] superior to the ones obtainable with LDA or GGA type functionals.[16,17] In particular, when OH groups are involved, large overestimation of the H bond strength and the related red shift of the OH stretching frequency affecting most of the other functionals[18,19] is avoided.

The level of accuracy in evaluating Coulomb and Hartree−Fock exchange series is controlled by five parameters,[24] for which standard values have been used (6 6 6 6 12).

The DFT exchange-correlation contribution is evaluated by numerical integration over the unit cell volume.[15] Radial and angular points of the atomic grid are generated through Gauss−Legendre and Lebedev quadrature schemes. A pruned grid has been adopted, as discussed in ref 15. The impact of the grid size on both the accuracy and the cost of a calculation has been discussed at length in previous papers.[15,17,28] However, since this system is larger that any other studied with the present computational schemes so far and because of the large anharmonic effects due to the presence of many hydrogen atoms in the unit cell, the importance of the grid size on energy, geometry, and frequencies has been checked again. In the following, the notation $(n_r,n_\Omega)p$ indicates a pruned grid of n_r radial points and n_Ω angular points on the Lebedev surface in the most accurate integration region. Three grids have been considered, namely, (55,434)*p*, (75,974)*p*, and (99,1454)*p*. The variability of the calculated vibration frequencies, ν_v, as depending on the integration grid is estimated through four global indices evalu-

TABLE 1: Dependence of the Calculated Vibration Frequencies of Katoite at Γ on t_E (SCF Convergence Tolerance), u (Atomic Displacement for the Numerical Evaluation of the Hessian from the Analytical Energy Gradients), and N (Number of Total Energy Calculations along Each Nuclear Cartesian Coordinate for the Evaluation of the Hessian Matrix)[a]

			$\overline{\lvert\Delta\rvert}$	$\bar{\Delta}$	Δ_{min}	Δ_{max}
t_E	10		0.6	−0.5	−2.8	0.9
		low	2.8	−2.8	−12.9	0.6
u	0.003	OH	11.4	11.4	10.7	12.0
		full set	4.0	−0.8	−12.9	12.0
		low	1.1	1.1	−0.6	4.8
N	2	OH	5.8	−5.8	−7.0	0.0
		full set	1.8	0.1	−7.0	4.8

[a] $\bar{\Delta}$, $\overline{\lvert\Delta\rvert}$, Δ_{max}, and Δ_{min} (all in cm^{-1}) are the average of the difference, the average of the absolute difference, and the maximum and minimum difference computed with reference to the frequencies evaluated with $t_E = 11$, $u = 0.001$ Å, and $N = 1$, respectively. For the three entries, only the indicated parameter has been modified with respect to the reference conditions. "low" and "OH" refer to frequencies below 1000 cm^{-1} and to the 48 OH stretching frequencies, respectively.

ated with respect to a reference set of M frequencies, ν_υ^{ref}, as follows (see Table 1):

$$\overline{\lvert\Delta\rvert} = M^{-1}\sum_{\upsilon=1}^{M}|\nu_\upsilon - \nu_\upsilon^{ref}|$$

$$\bar{\Delta} = M^{-1}\sum_{\upsilon=1}^{M}\nu_\upsilon - \nu_\upsilon^{ref}$$

$$\Delta_{max} = \max(\nu_\upsilon - \nu_\upsilon^{ref})$$

$$\Delta_{min} = \min(\nu_\upsilon - \nu_\upsilon^{ref}) \qquad \upsilon = 1, 2, \ldots, M$$

Even the smallest grid considered here provides good results for energy and equilibrium geometry as well as for frequencies (average absolute error with respect to the largest grid of only 3 cm^{-1}). However, as one frequency differs by more than 20 cm^{-1} with respect to better grids, we prefer to use the (75,-974)*p* grid, providing essentially the same quality of results for all properties as the largest grid which is much more expensive.

The reciprocal space was sampled according to a regular sublattice with a shrinking factor, IS, equal to 2, corresponding to the choice of three independent k vectors in the irreducible Brillouin zone; the use of such a small IS value is justified by the large size of the unit cell.

The gradient with respect to the atomic coordinates is evaluated analytically.[29−31] Equilibrium atomic positions are determined[32] by using a modified conjugate gradient algorithm as proposed by Schlegel.[33] Convergence in the geometry optimization process is tested on the root mean square (rms) and the absolute value of the largest component of both the gradients and the nuclear displacements. The thresholds for the maximum and the rms forces and the maximum and the rms atomic displacements on all atoms have been set to 0.000 045, 0.000 030 and 0.000 180, 0.000 120 au, respectively. Such strict tolerances provide an accurate definition of the equilibrium geometry that is adequate for the calculation of frequencies. Optimization is considered complete as soon as the four conditions are simultaneously fulfilled.

In regard to the calculation of frequencies, we refer to a previous paper[15] for a more explicit formulation of the method, here simply reminding the reader that frequencies at the Γ point have been obtained within the harmonic approximation by diagonalizing the mass-weighted Hessian matrix, **W**, whose (i, j) element is defined as $W_{ij} = H_{ij}/\sqrt{M_i M_j}$, where M_i and M_j are the masses of the atoms associated with the i and j coordinates, respectively.

Once the Hessian matrix, **H**, has been calculated, frequency shifts due to isotopic substitutions can be calculated readily, at no cost, by exchanging masses in the above formula. In the present case, isotopic effects have been estimated by substituting ^{42}Ca for ^{40}Ca, ^{29}Al for ^{27}Al, ^{18}O for ^{16}O, and D for H. Although the natural abundance of ^{27}Al is 100%, so that ^{29}Al cannot be used in experiments, isotopic substitution is used here as an effective tool for identifying the ions contributing to the modes in a given frequency range. Alternatively, sets of atoms have been assigned infinite mass, so that the vibration of a fragment can be isolated without affecting the crystalline environment.

Energy first derivatives with respect to the atomic positions, $\upsilon_j = \partial V/\partial u_j$, are calculated analytically for all u_j coordinates (u_j is the displacement coordinate with respect to equilibrium), whereas second derivatives at $\mathbf{u} = 0$ are calculated numerically using a single displacement along each coordinate ($N = 1$):

$$\left[\frac{\upsilon_j}{u_i}\right]_0 \approx \frac{\upsilon_j(0, \ldots, u_i, \ldots)}{u_i}$$

or averaging two displacements ($N = 2$):

$$\left[\frac{\upsilon_j}{u_i}\right]_0 \approx \frac{\upsilon_j(0, \ldots, u_i, \ldots) - \upsilon_j(0, \ldots, -u_i, \ldots)}{2u_i}$$

The influence of either the number of points used in the evaluation of the second derivatives ($N = 1, 2$), or the magnitude of the displacement, u_i, of each atomic coordinate ($u = 0.001$, 0.003 Å for all atoms) on the calculated frequencies has been checked. Both parameters can be considered a measure of (i) numerical noise in the calculation and (ii) departure of the potential energy surface along the atomic Cartesian coordinates from harmonic behavior. Previous calculations on α-quartz[15] and $CaCO_3$[28] have shown that the influence of both u and N on our statistical indices is very small. For example, $\overline{\lvert\Delta\rvert}$ is always smaller than 1 cm^{-1} (see Table 3 in ref 15 and the Computational Details section in ref 28), but we can argue that the much larger effect of u and N in the present case (see "full set" row in Table 1) is mainly related to anharmonicity effects due to the presence of 48 hydrogen atoms in the unit cell. For this reason, the OH stretching modes (OH row in the table) have been separated from the other modes, because they are affected by large anharmonicity[17,18] (150 cm^{-1} or more), which explains the large dependence of harmonic frequencies on u and N. The effect of u and N on modes below 1000 cm^{-1} is much smaller ($\overline{\lvert\Delta\rvert}$ = 2.8 and 1.1 cm^{-1}) but not as negligible as that for other systems, indicating that the potential energy surface (PES) is not as quadratic near the minimum as in other cases. Other modes involving hydrogen (bending or "rotations") are probably slightly anharmonic, too. This is confirmed by the results of our very recent study of pyrope garnet,[34] $Mg_3Al_2Si_3O_{12}$, having the same structure as katoite but no hydrogen atoms. In this case (see Table 3 in ref 34), $\overline{\lvert\Delta\rvert}$ is 0.4 and 0.1 cm^{-1} for the same change in u and N, respectively.

Since the energy variations for the displacements here considered can be as small as 10^{-6}−10^{-8} hartree, the tolerance on the convergence of the self-consistent field (SCF) cycles has

been set to 10^{-11} hartree. The effect of using a less severe tolerance (10^{-10} hartree) is shown in the first line of Table 1.

The above procedure generates only the TO modes for an ionic compound. A correction should be added to the Hessian in order to obtain the transverse optical (TO)−longitudinal optical (LO) splitting for the F_{1u} modes.[15] However, such a correction was not considered in the present study.

Anharmonic OH stretching frequencies have been calculated as described in previous papers.[17,35] Anharmonicity constant and harmonic OH stretching frequency have been computed from the first vibrational transitions ω_{01} and ω_{02} obtained by solving the one-dimensional Schroedinger equation numerically:

$$\omega_e x_e = (2\omega_{01} - \omega_{02})/2$$

$$\omega_e = \omega_{01} + 2\omega_e x_e$$

Visualization of structures has been dealt with the MOLDRAW program,[36,37] and molecular drawings have been rendered by the PovRay program using input files prepared by MOLDRAW.

III. Results

The highly symmetric katoite structure contains all 48 point symmetry operations of the $m\bar{3}m$ group. Decomposition of the reducible representation built on the basis of the Cartesian coordinates of the unit cell atoms leads to the following symmetry assignment of the 348 normal modes (this analysis is performed automatically by the CRYSTAL code):

$$\Gamma_{total} = 6A_{1g} + 7A_{2g} + 13E_g + 21F_{1g} + 20F_{2g} + 7A_{1u} + 8A_{2u} + 15E_u + 24F_{1u} + 23F_{2u}$$

In total, 23 IR (F_{1u}) and 39 Raman ($6A_{1g} + 13E_g + 20F_{2g}$) modes are expected to exist. All remaining modes are inactive. One of the F_{1u} modes (in the following, we will also indicate the set of two or three degenerate modes corresponding to a given vibration frequency as "one mode") is acoustic in character, and its frequency is to be zero at the Γ point, corresponding to pure translation. From diagonalization of the full Hessian matrix, its frequency results to be 0.5 cm^{-1}, with the small deviation from zero being a further measure of the numerical accuracy of the method.

As for the experimental vibrational investigation of Si-free katoite, two sets of results are available: the IR work by Rossman[4] that explores the zone of the OH stretching only at room temperature and the IR and Raman work by Kolesov and Geiger[38] at both low (4 K) and room temperatures (298 K), covering a much wider range of the spectrum (from 163 to 3861 cm^{-1}). In the following, we will provide and discuss the full ab initio calculated spectrum and carry out a comparison with experimental IR and Raman spectra by Kolesov and Geiger[38] at the end of our analysis.

Katoite presents many peculiar features that are expected to influence its vibrational spectrum strongly:

(1) The presence of so many hydrogen atoms breaks connectivity between polyhedra (see Figure 1), which is typical of isostructural garnets such as grossular.

(2) Three different kinds of bonds are present in katoite, namely, a strong covalent bond (O−H), a partially covalent bond (Al−O), and a fully ionic bond (Ca−O).

(3) Hydrogen mass is much smaller than that for all other atoms.

As a consequence, katoite can be represented as a set of Al-$(OH)_6$ octahedral anions loosely linked by compensating Ca cations. This view is supported by the appearance of signals at very low frequencies (around 60 cm^{-1}, i.e., about one-third of the lowest frequencies in grossular),[39,40] because part of the system can translate or rotate with very low energy within the unit cell. We will then focus our attention on the $Al(OH)_6$ octahedra (see Figure 2a for a representation of the primitive cell). The content of the colored cube in Figure 2a is represented in more detail in Figure 2b, showing that the octahedron at the center of the cube can interact with eight octahedra at the vertices. Rotation and translation of each octahedron is hindered or favored by the other octahedra and Ca cations.

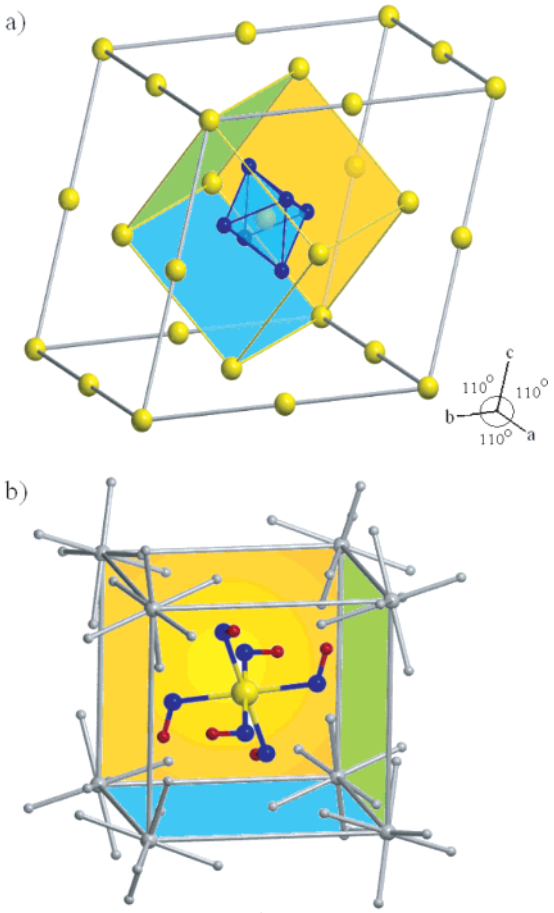

Figure 2. (a) Primitive cell of katoite with representation of the central AlO_6 octahedron only and Al atoms. (b) Details of the colored cube in part a, with full representation of the central octahedron, whereas its eight nearest neigbors are only sketched. The Al−Al, O−O, and H−H shortest distances between different octahedra are 5.48, 3.29, and 1.93 Å, respectively.

We can then attempt to classify the full set of modes (348) in terms of rotations, translations, and inner modes of the octahedra:

(1) Translations of the Ca cations (36)
(2) Translations of the octahedra (24)
(3) Rotations of the octahedra (24)
(4) OH stretching modes (48)
(5) OH bending modes (48)
(6) Rotations of H around the Al−O axis (48)
(7) The remaining modes of the octahedra (120 = 7 atoms/octahedron × 8 octahedra × 3 coordinates − 24 rotations − 24 translations).

Such a partition is arbitrary at some extent and must be used with caution, as coupling among the different categories listed above does occur. This is confirmed in Table 2 by the continuum of modes in the 60−1000 cm^{-1} range of the spectrum,

TABLE 2: Full Set of Katoite Vibrational Modes and Effect of the ^{44}Ca, ^{29}Al, ^{18}O, and D Isotopic Substitution[a]

		$Ca_3Al_2[(OH)_4]_3$	^{44}Ca	^{29}Al	^{18}O	D			$Ca_3Al_2[(OH)_4]_3$	^{44}Ca	^{29}Al	^{18}O	D
	label	ν	$\Delta\nu$	$\Delta\nu$	$\Delta\nu$	$\Delta\nu$		label	ν	$\Delta\nu$	$\Delta\nu$	$\Delta\nu$	$\Delta\nu$
F_{2u}	4−6	60.5					F_{2u}	180−182	431.5	−1.0	−3.4	−15.7	−44.0
F_{1u}	7−9	**67.0**					F_{1u}	183−185	**440.3**		−3.2	−14.2	−34.9
B_u	10−10	67.3					E_u	186−187	447.2			−18.1	−48.7
F_{1g}	11−13	87.8					E_g	188−189	**451.2**			−18.7	−35.7
B_g	14−14	109.1	−2.2			−13.2	F_{1g}	190−192	454.1			−14.7	−51.7
F_{1u}	15−17	**113.8**		−1.0			F_{2u}	193−195	459.0			−21.5	−32.6
E_g	18−19	**114.1**			−4.7	−14.7	A_u	196−196	469.4		−2.7	−21.7	−15.6
E_u	20−21	116.3		−1.0	−4.0		F_{1u}	197−199	**487.9**		−8.1	−12.3	
F_{1g}	22−24	128.6	−2.7		−4.1		F_{2u}	200−202	503.6		−7.0	−14.3	−51.3
F_{2g}	25−27	**150.9**	−3.1		−5.2		A_g	203−203	**503.8**			−14.1	−62.0
F_{2u}	28−30	155.6	−1.7	−1.5	−4.6		E_u	204−205	518.8		−8.1	−16.3	−50.6
B_u	31−31	157.7	−4.1			−24.5	F_{1u}	206−208	**519.3**		−8.5	−14.5	
F_{2g}	32−34	**163.4**			−8.7		F_{1g}	209−211	530.6			−27.9	−35.1
F_{1g}	35−37	164.0	−3.6		−4.3	−16.6	F_{2u}	212−214	531.3		−7.7	−5.8	−47.2
F_{1u}	38−40	**164.0**	−5.7				F_{2g}	215−217	**540.8**			−28.9	−30.3
E_u	41−42	164.2	−1.7	−1.6	−4.5		B_g	218−218	542.4			−29.6	−14.3
E_g	43−44	**166.4**	−5.3				F_{1u}	219−221	**544.2**		−7.1	−16.4	−17.1
F_{2g}	45−47	**179.2**	−2.1		−6.6		B_u	222−222	544.3		−6.1	−17.7	−20.1
F_{2u}	48−50	184.8	−3.6		−6.1		F_{2u}	223−225	546.2		−7.0	−13.5	−15.8
F_{1g}	51−53	187.0	−4.0		−4.9		E_u	226−227	547.8		−2.3	−6.8	−31.2
F_{1g}	54−56	193.9	−7.1				A_g	228−228	**559.4**			−28.4	−14.3
E_u	57−58	195.5	−4.2				A_u	229−229	583.4		−9.1	−15.0	−46.2
F_{1u}	59−61	200.2	−6.2			−15.3	F_{1g}	230−232	652.4			−4.2	−125.6
B_g	62−62	200.3	−2.6		−8.1		F_{2u}	233−235	654.6		−3.7	−8.0	−103.2
F_{2u}	63−65	208.6	−3.5		−5.2	−15.1	E_u	236−237	656.7	−1.2	−9.8	−13.1	−34.1
F_{2u}	66−68	212.1	−2.5		−4.9		E_g	238−239	**698.2**				−173.4
F_{1u}	69−71	**218.1**	−3.3		−5.1	−20.2	A_u	240−240	756.8				−185.6
B_u	72−72	218.5			−10.5		F_{2g}	241−243	**757.0**				−192.1
F_{1g}	73−75	221.4	−5.1		−5.1	−10.8	F_{1u}	244−246	**766.5**		−1.0		−192.8
F_{2g}	76−78	**227.6**	−6.6		−5.8	−16.5	F_{2u}	247−249	768.7		−1.2		−184.4
E_u	79−80	232.2	−2.4		−5.8	−21.9	F_{2g}	250−252	**782.1**				−212.7
A_u	81−81	232.6		−2.8	−9.2		F_{2g}	253−255	**798.1**				−203.6
F_{2u}	82−84	232.9	−2.8		−9.5		F_{1g}	256−258	808.7				−210.1
F_{1u}	85−87	**237.9**			−11.1	−17.2	F_{2u}	259−261	816.6		−1.2		−179.6
F_{1u}	88−90	**244.0**	−4.1		−5.2	−14.0	F_{1u}	262−264	**820.6**				−197.3
A_g	91−91	**244.1**			−13.6		F_{2g}	265−267	**838.2**			−4.6	−201.8
F_{2g}	92−94	**246.7**	−5.8			−20.2	E_g	268−269	**868.4**				−232.7
F_{1g}	95−97	247.6			−10.4	−23.3	F_{1g}	270−272	868.4			−6.3	−201.3
E_g	98−99	**250.4**	−2.8		−8.8	−20.6	F_{2u}	273−275	868.9		−2.8	−4.9	−185.6
F_{2u}	100−102	259.4	−2.7		−8.9		F_{1u}	276−278	**886.8**		−1.9	−5.1	−196.0
F_{1u}	103−105	**269.2**			−10.8	−28.3	E_u	279−280	907.1		−1.1		−220.5
F_{2g}	106−108	**276.7**	−1.5		−7.2	−19.0	F_{1g}	281−283	936.9				−242.5
B_g	109−109	280.8	−4.0			−45.7	B_u	284−284	940.0		−1.3		−228.9
F_{1u}	110−112	**281.5**	−1.7		−8.1	−11.1	A_u	285−285	954.4		−1.1		−229.0
B_u	113−113	299.0	−3.1		−6.6	−25.4	F_{2g}	286−288	**955.8**			−4.3	−238.7
E_g	114−115	**299.6**			−10.2	−28.3	A_g	289−289	**956.7**				−251.2
A_u	116−116	300.8			−15.5	−10.3	F_{1u}	290−292	**957.3**		−1.0		−236.5
F_{1g}	117−119	301.2	−1.3		−8.4	−47.4	E_g	293−294	**958.3**				−248.6
F_{2u}	120−122	308.7		−1.7	−13.2	−16.5	B_g	295−295	965.9			−5.1	−240.6
E_u	123−124	311.5			−14.9	−18.9	F_{2u}	296−298	968.5		−1.2	−4.2	−221.1
F_{1u}	125−127	**322.6**			−11.3	−21.3	E_u	299−300	993.8				−250.5
F_{2u}	128−130	328.4			−13.4	−21.5	B_u	301−301	3841.9			−12.6	−1035.9
E_g	131−132	**332.8**			−17.4		F_{2u}	302−304	3842.7			−12.6	−1036.4
F_{1g}	133−135	333.4			−15.7	−23.1	F_{1g}	305−307	3842.9			−12.6	−1036.6
F_{1g}	136−138	347.5			−18.6	−14.7	F_{1u}	308−310	**3843.6**			−12.6	−1036.9
E_u	139−140	350.2		−1.9	−11.3	−41.3	F_{1g}	311−313	3844.1			−12.6	−1036.9
F_{2g}	141−143	**356.8**			−17.0	−18.6	E_g	314−315	**3844.2**			−12.7	−1036.8
F_{1g}	144−146	367.2			−12.7	−23.5	F_{2g}	316−318	**3846.7**			−12.6	−1037.8
A_g	147−147	**371.7**			−11.9	−77.0	F_{1u}	319−321	**3847.0**			−12.5	−1038.6
F_{2g}	148−150	**373.5**			−18.3	−29.8	E_u	322−323	3848.4			−12.5	−1038.7
B_g	151−151	382.9			−16.4	−30.5	F_{1g}	324−326	3850.7			−12.4	−1039.5
E_u	152−153	387.9		−1.0	−17.0	−21.1	F_{2u}	327−329	3851.2			−12.4	−1039.9
F_{1u}	154−156	**388.3**		−2.6	−9.9	−44.4	F_{2g}	330−332	**3851.4**			−12.4	−1039.9
F_{2g}	157−159	**396.5**			−22.0		F_{2u}	333−335	3851.6			−12.4	−1040.0
F_{2u}	160−162	399.7		−1.5	−16.9	−30.9	A_g	336−336	**3851.9**			−12.5	−1039.7
F_{1u}	163−165	**407.0**		−4.0	−15.0	−25.3	B_g	337−337	3854.8			−12.4	−1040.8
F_{2g}	166−168	**409.4**			−21.2	−20.1	E_u	338−339	3856.8			−12.3	−1042.4
E_g	169−170	**413.0**			−22.2	−19.1	F_{1u}	340−342	**3858.0**			−12.3	−1042.8
F_{2g}	171−173	**416.7**			−18.7	−17.3	E_g	343−344	**3860.1**			−12.2	−1043.6
F_{1g}	174−176	419.6			−20.1	−30.5	F_{2g}	345−347	**3860.7**			−12.3	−1043.1
E_g	177−178	**420.8**			−21.6	−16.4	A_u	348−348	3861.9			−12.4	−1042.6
B_u	179−179	422.3		−6.6	−11.5	−18.1							

[a] Isotopic shifts smaller than 1 (Ca and Al), 4 (O), and 10 (D) cm^{-1} are not reported. Bold numbers indicate IR and Raman active frequencies. ν and $\Delta\nu$ are in cm^{-1}.

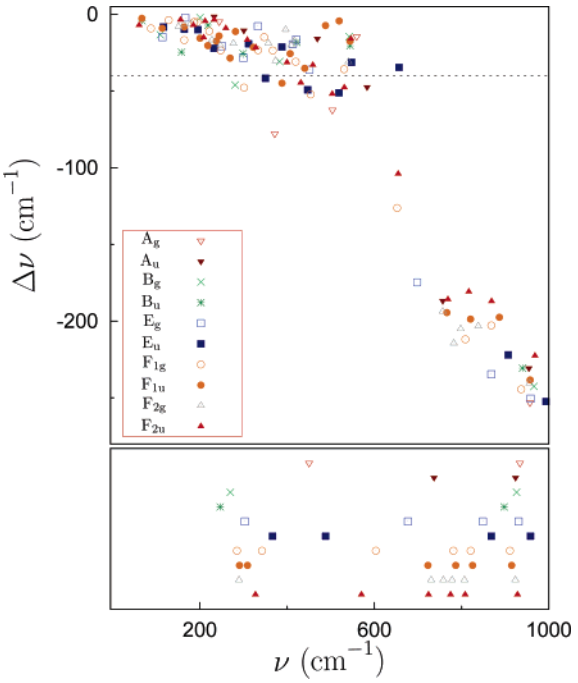

Figure 3. (top) Shift ($\Delta\nu$) of vibrational frequencies (ν) in katoite when deuterium is substituted for hydrogen. Only frequencies below 1000 cm^{-1} are reported. The dotted line isolates the 96 modes with larger D isotopic shift. (bottom) Frequencies obtained by "freezing" all atoms in the unit cell except the 48 H atoms ($S_{H_{48}}$ model) (the number of modes reported in the figure is $2 \times 48 = 96$, as the remaining 48 stretching modes are observed at much higher frequencies). To avoid superposition of symbols, vibration frequencies are displayed along rows, with each row corresponding to modes of a given symmetry, so that the vertical axis does not represent isotopic shift in the bottom figure. From a comparison of the top and bottom figures, a similar frequency distribution of the 96 H modes results in the full katoite spectrum and for the $S_{Al(OH)_6}$ model.

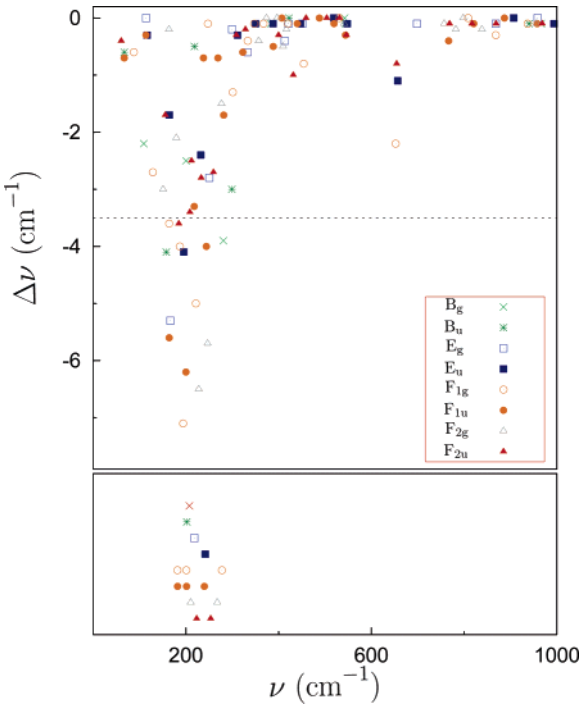

Figure 4. (top) Isotopic effect of ^{44}Ca (substituting ^{40}Ca) on the vibration frequencies of katoite. The dotted line isolates the 36 modes with larger Ca isotopic shift. (bottom) Vibration frequencies obtained by freezing all of the atoms in the unit cell except the 12 Ca atoms (the S_{Ca} model, 36 modes); vibration frequencies are displayed along rows, with each row corresponding to modes of a given symmetry. From a comparison between the top and bottom figures, a similar frequency distribution of Ca-like modes results in the full katoite spectrum and for the S_{Ca} model.

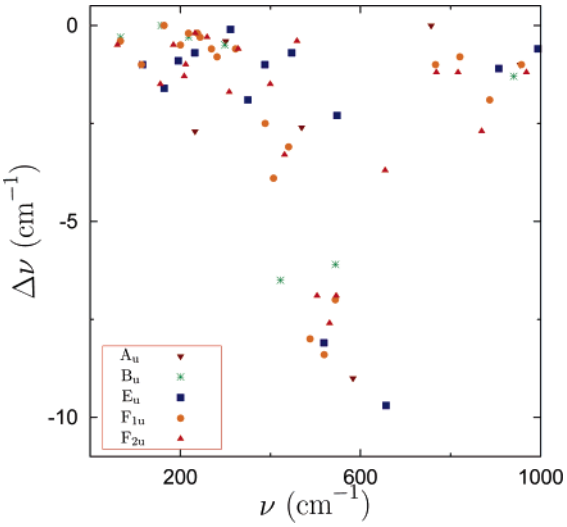

Figure 5. Isotopic effect of substituting ^{29}Al for ^{27}Al on vibration frequencies of katoite.

corresponding to modes of groups 1−3 and 5−7 in the above list. On the contrary, OH stretching modes appear at much higher frequencies and they will be discussed in a separate section.

To understand the nature of modes in the 60−1000 cm^{-1} range, a few complementary tools have been used:

(1) Isotopic substitution, whose effects are listed in Table 2 and shown in Figures 3−6. By supposing that the isotopic shift is proportional to the participation of a given atom in a mode, the "hydrogen region" (650−993 cm^{-1}), the "aluminum region" (400−650), and the "calcium region" (150−300) are located easily in the figures. In regard to oxygen, shifts are very low both in the hydrogen region, above 650 cm^{-1}, and below 300 cm^{-1}, whereas most shifts are larger than 10 cm^{-1} in the intermediate zone (300−650 cm^{-1}), suggesting that there is a large participation of oxygen in modes of group 7 (AlO_6 modes).

(2) Decomposition of the spectrum into subunits. This can be attained by freezing atoms which are not part of a subunit, as if they had an infinite mass (in practice, isotopic substitution of atoms with a very large mass). In this way, steric, electrostatic, and short range repulsion effects, as well as symmetry of the crystalline environment, which would be lost in an isolated fragment, are preserved, but the spectrum retains only those modes of the fragment we are interested in, that is fully decoupled from the rest of the crystal. In the following, four kinds of subunits will be considered: (i) one isolated $Al(OH)_6$ octahedron ($S_{Al(OH)_6}$), (ii) H_6, that is, the H atoms only of the $Al(OH)_6$ octahedron (S_{H_6}), (iii) all 48 hydrogens in the unit cell ($S_{H_{48}}$), and (iv) all Ca ions (S_{Ca}).

(3) Animations for some of the vibrational modes are available at the CRYSTAL website.[41] To make the animation as clear as possible, only a fraction of the unit cell is displayed, containing one AlO_6 octahedron and six of eight octahedra at the vertices of the cube around it, plus Ca ions when they are involved in the mode.

We now analyze the OH stretching band, before discussing the vibrational properties of a single octahedron.

A. OH Stretching Band. The OH stretching band consists of 48 modes corresponding to different coupling of the 48 OH stretching oscillators in the unit cell (only 20 frequencies are

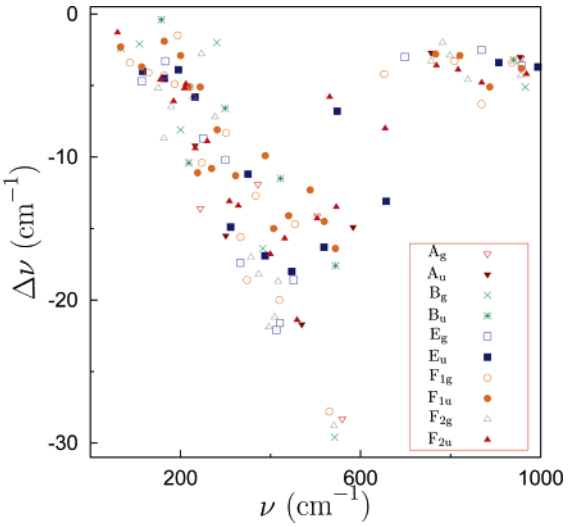

Figure 6. Isotopic effect of substituting ^{18}O for ^{16}O on vibration frequencies below 1000 cm^{-1}.

actually observed because of degeneracies). At zero pressure, OH oscillators are fully decoupled both from the rest of the crystal and from each other because the large distance between the H and O atoms of neighboring OH groups (2.51 Å) prevents any hydrogen bond in the $(OH)_4$ defect from forming. Consequently, the 20 calculated harmonic frequencies span a small range from 3842 (B_u) to 3862 (A_u) cm^{-1}, with the fully symmetric A_g mode at the center of the band. Three modes, in a range of just 15 cm^{-1}, at 3844, 3847, and 3858 cm^{-1}, correspond to IR active modes (F_{1u} symmetry), whereas six modes are Raman active, of which three are of F_{2g} symmetry (3847, 3851, and 3861 cm^{-1}), two are of E_g symmetry (3844 and 3860 cm^{-1}), and one is of A_g symmetry (3852 cm^{-1}).

To compare our calculated data with experiment, anharmonicity must be taken into account. As was anticipated in the computational section, all 48 OH bond lengths have been varied in phase (A_g symmetry, at 3852 cm^{-1} in the harmonic spectrum). The resulting ω_{01}(OH) frequency is 3673 cm^{-1}, with an anharmonic constant, $\omega_e x_e$, of 86 cm^{-1}. By replacing H in 47 of the 48 OH groups in the unit cell with D, the symmetry reduces to *P*1 and the remaining OH group is fully decoupled from the rest of the crystal. However, its harmonic frequency is 3852 cm^{-1}, essentially at the center of the IR band, and the corresponding anharmonic frequency is 3682 cm^{-1}, that is, only 9 cm^{-1} higher than the fully symmetric A_g mode, thus confirming an extremely low coupling of different OH oscillators.

B. Al(OH)$_6$ Octahedron, Hydrogen Bending, and Rotation Modes. The interpretation of the katoite spectrum in the range 60−1000 cm^{-1} is a difficult task because of the large number of modes and complexity of vibration patterns. As anticipated above, decoupling one $Al(OH)_6$ octahedron from the rest of the unit cell can be very informative about the separability of the various group vibrations. The calculated vibration frequencies for $S_{Al(OH)_6}$ are reported in Table 3 (animations available at the CRYSTAL website).[41] Symmetry labels refer now to the subgroup of this subsystem ($\bar{3}$), characterized by a 3-fold improper axis oriented along the diagonal of the cube and crossing opposite triangular faces of the octahedron. As $S_{Al(OH)_6}$ contains only 13 atoms free to vibrate, there are 39 degrees of freedom. Modes can be classified according to six of the seven categories listed in the previous section, with the Ca ions being frozen:

1. Translations (3)
2. Rotations (3)
3. OH stretching (6)
4. OH bending (6)
5. H rotations about the Al−O axis (6)
6. Modes of the AlO_6 group (15)

The full spectrum of katoite results from coupling of these modes to the modes of the other octahedra, after addition of the Ca modes. Thus, we can try to link the full spectrum to that of $S_{Al(OH)_6}$. The interesting point is that the various categories are well separated in the free octahedron spectrum ($S_{Al(OH)_6}$) and classification is relatively simple.

The six OH stretching modes form a narrow band (only 4 cm^{-1} wide) exactly at the center of the band of the full system.

The six modes between 802 and 867 cm^{-1} correspond to OH bending (the band is 65 cm^{-1} wide) and the six modes with frequencies between 553 and 669 cm^{-1} to rotations of H around the Al−O axis (this band is as large as 116 cm^{-1}). This assignment on the basis of mode animations[41] is also confirmed by isotopic substitutions, as reported in Table 3. In fact, no shift for aluminum is observed in either set and, in regard to oxygen, there is a small shift for bending and essentially no shift for rotations. Following this analysis, the six modes that we classify as "H rotations" are pure H motions essentially not involving either Al or O atoms.

We can freeze our fragment further by increasing the mass of all atoms to infinity except the six H's in the octahedron (S_{H_6} model). In S_{H_6}, there are only 18 modes left, namely, H stretching, bending, and rotations, with the shift from the corresponding frequencies of $S_{Al(OH)_6}$ depending on the participation of the other atoms to the vibration. The data reported in the fourth column of Table 3 show that OH stretching frequencies are shifted by about 100 cm^{-1} (compare columns 3 and 4), as a consequence of the small but non-null participation of oxygen in the definition of the reduced mass. OH bending modes red-shift by a smaller amount (30−50 cm^{-1}), as a consequence of the smaller participation of oxygen, as documented by an isotopic shift of just 4−6 cm^{-1}, whereas it was 12 cm^{-1} for stretching (Table 3). H rotation modes shift by only 4−11 cm^{-1}, confirming their nearly pure H character.

The H rotation band deserves a few more comments:

(1) There is a large gap (130 cm^{-1}) between the H bending and rotation modes.

(2) The separation between the lowest mode in the H rotation band and Al−O modes is only 6 cm^{-1}.

(3) The three higher frequency modes at 663 and 669 cm^{-1} are separated from the remaining three modes by 60 cm^{-1}, with the gap between the lower frequencies being about 40 cm^{-1}.

(4) All H rotation modes show very similar Al and O isotopic shifts. On the contrary, they differ in H isotopic shift dramatically, with this being similar to the shift of bending modes for the modes at 663 and 669 cm^{-1}, whereas it is much smaller for the other three modes. If this behavior applies also to the full katoite spectrum, 72 modes (48 bending plus 24 H rotations) with H isotopic shifts larger than 150 are expected to exist, and this is actually the case (in fact, they are only 69, from mode n. 230 to 300, and excluding modes n. 236−237 in Table 2). The large difference in frequency and isotopic shift between the two sets of H rotation modes is a consequence of relative rotation, as can be appreciated in Figure 7, where it is clear that when two H atoms along a given axis rotate counterclockwise, the energy required is higher, as well as the H isotopic shift (Table 3).

TABLE 3: Vibrational Modes of the Isolated $Al(OH)_6$ Octahedral Fragment (39 Modes) Vibrating in the Field of the Frozen Crystal ($S_{Al(OH)_6}$ Model) and Effect of the ^{29}Al, ^{18}O, and D Isotopic Substitution[a]

			$S_{Al(OH)_6}$	S_{H_6}	^{29}Al	^{18}O	D
assigment	symmetry	label	ν	ν	$\Delta\nu$	$\Delta\nu$	$\Delta\nu$
octahedron	E_u	1−2	163.8		−1.9	−6.3	−3.2
translation	A_u	3	194.7		−1.6	−8.6	−2.3
octahedron	A_g	4	198.3		0.0	−11.2	−1.9
rotation	E_g	5−6	200.4		0.0	−10.9	−5.2
AlO_6 modes	A_u	7	264.5		−0.1	−14.4	−7.5
	E_u	8−9	286.8		−0.1	−15.3	−10.9
	E_g	10−11	357.0		0.0	−18.9	−17.4
	A_g	12	374.9		0.0	−18.8	−26.7
	E_g	13−14	398.9		0.0	−22.2	−7.2
	E_u	15−16	400.0		−1.7	−17.8	−24.4
	A_u	17	423.3		−4.8	−15.9	−22.0
	E_u	18−19	524.5		−9.0	−12.9	−101.3
	A_g	20	538.4		0.0	−29.4	−142.3
	A_u	21	547.9		−7.7	−15.2	−61.7
H rotation	A_g	22	553.5	549.6	0.0	−0.6	−33.3
	E_u	23−24	599.5	590.4	−0.2	−2.0	−71.1
	E_g	25−26	662.9	658.1	0.0	−0.6	−187.1
	A_u	27	669.2	656.9	−0.2	−1.5	−145.3
H−O−Al bending	E_g	28−29	802.5	770.5	0.0	−4.2	−200.4
	A_u	30	825.4	787.8	−1.2	−3.6	−185.8
	E_u	31−32	855.5	795.0	−1.8	−5.2	−190.2
	A_g	33	867.7	820.6	0.0	−6.4	−199.2
OH stretching	A_u	34	3847.8	3735.2	0.0	−12.5	−1038.1
	E_g	35−36	3849.4	3736.4	0.0	−12.5	−1039.1
	E_u	37−38	3850.7	3738.5	0.0	−12.4	−1039.9
	A_g	39	3851.4	3739.6	0.0	−12.4	−1039.5

[a] In column 4, the 18 modes of the H_6 subunit of $S_{Al(OH)_6}$ (the S_{H_6} model) are reported. ν and $\Delta\nu$ are in cm^{-1}.

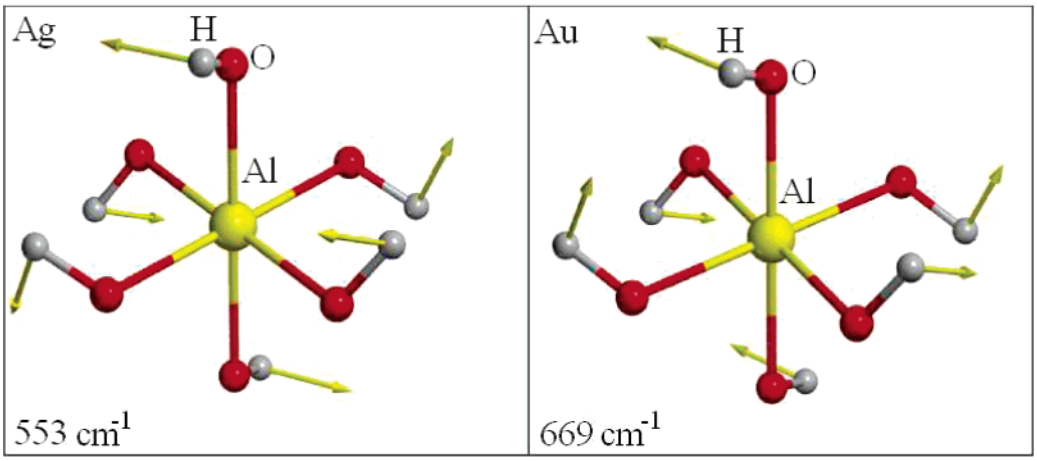

Figure 7. Representation of the eigenvectors associated with rotations of H atoms around an O−Al axis. Symmetry and frequency values refer to the spectrum of a single octahedron obtained by freezing all other atoms in the unit cell ($S_{Al(OH)_6}$). Note the large frequency difference between A_g (the two H atoms along the O−Al−O axes rotate in the same direction) and A_u (opposite rotation direction) modes.

We continue our analysis with the 15 inner modes of the Al−O_6 group, which form by far the largest band, ranging from 264 to 548 cm^{-1}. As mentioned above, it nearly overlaps the H rotation band. The remaining three translations (164 and 195 cm^{-1}) and rotations (198 and 200 cm^{-1}) are almost pure modes, although only 60 cm^{-1} separate them from the Al−O_6 modes (see also the CRYSTAL website).[41]

In the full katoite spectrum, the gap between H bending and rotation of $S_{Al(OH)_6}$ vanishes (Table 2). Symmetry analysis can be used to verify whether the two bands (H bending and rotation) simply form a continuum without mixing or overlap to a large amount. The 48 H bending modes generate a reducible representation whose composition is as follows:

$$\Gamma_{rid} = A_{1g} + A_{2g} + 2E_g + 3F_{1g} + 3F_{2g} + A_{1u} + A_{2u} + 2E_u + 3F_{1u} + 3F_{2u}$$

where each irreducible representation appears a number of times equal to its dimensionality, with this being a property of all of the objects in the cell having the full multiplicity of any general position, such as vectors representing the OH stretching, bending, and H rotation. If the two bands do not mix, we should find first (from high frequencies down to low frequencies) the full set of modes corresponding to $\Gamma_{rid}^{bending}$ and then the $\Gamma_{rid}^{rotation}$ modes. The 48 modes labeled 253−300 in Table 2 match the decomposition of Γ_{rid} exactly (for example, F_{1g} appears three times, and E_g appears twice, and so on). This cannot be considered as an absolute proof of full separation of the bending modes from the remainder of the spectrum, as some rotation might be exchanged with a bending with the same symmetry, but this event seems unlikely for more than one or two modes and close inspection of the animations confirms that actually this is not the case. In summary, the gap separating H bending

and rotation bands in $S_{Al(OH)_6}$ (see Table 3) disappears in the full spectrum of katoite, but the two bands essentially do not overlap. In the full katoite spectrum, the bending and rotation bands spread out with respect to $S_{Al(OH)_6}$. Because of large mixing with the Al−O modes, the lower limit of the H rotation band (at 553 cm^{-1} in the isolated octahedron, Table 3) is not as clearly defined as the upper limit of the bending band at 993 cm^{-1}.

To assess the extension of the H rotation band in the low frequency region, we consider the $S_{H_{48}}$ model. The resulting frequencies ($48 \times 3 = 144$) cover the full spectrum from OH stretching down to 240 cm^{-1}, thus overlapping the modes involving Al and O atoms, as well as Ca motions (see below). Large mixing of the H rotation band with AlO_6 modes is not surprising, if we recall that only 6 cm^{-1} separates the lowest H rotation mode from the highest mode of the Al−O group (at 547.9 cm^{-1}) in $S_{Al(OH)_6}$ (Table 3). The involvement of the Al−O in the mode at 547.9 cm^{-1} is clearly revealed by the isotopic shift of Al (the second largest one) and oxygen (15 cm^{-1}, to be compared to 0.6 for the H rotation mode at 553.5). Such a tiny separation of 6 cm^{-1} is to be expected to vanish in the full system. In summary, in the katoite spectrum, the H rotation band forms a continuum with the OH bending band on the high frequency side, and it certainly overlaps the Al−O band on the low frequency side. Red shift with respect to $S_{Al(OH)_6}$ can be as large as 300 cm^{-1} (from 553 to 240 cm^{-1}). 240 cm^{-1}, as obtained with the $S_{H_{48}}$ model, is to be considered an upper limit, and actually, Table 2 shows that H isotopic shifts larger than 10 cm^{-1} can be found also at very low frequencies down to 109 cm^{-1}.

As a final comment, isotopic shift is very effective in discriminating modes, but some caution is necessary in the analysis. For example, Table 3 shows that there is a large H isotopic shift for the modes at 524 and 538 cm^{-1}, that are certainly Al−O octahedron modes, meaning that large H isotopic shift does not necessarily imply nearly pure H motion. In fact, when extended to Al (see the large shift for modes 18−19) and O (29 cm^{-1} is the largest oxygen shift), isotopic shift analysis permits a clear assignment of these modes to Al−O stretching (see also animations).[41]

C. The 60−300 cm^{-1} Range in the Spectrum. The low frequency portion of the spectrum is expected to contain Ca "translation" modes, as well as translations and rotations of the $Al(OH)_6$ octahedra, possibly with contributions from inner Al−O_6 and H rotation modes.

We can begin our analysis by looking at the Ca contribution. The coordinates of the 12 Ca atoms in the unit cell form the basis of a representation that consists of the following irreducible representations:

$$\Gamma_{Ca} = B_g + B_u + E_g + E_u + 3F_{1g} + 3F_{1u} + 2F_{2g} + 2F_{2u}$$

If all of the atoms of the unit cell except the 12 Ca cations are "frozen" (the S_{Ca} model described above), a very narrow spectrum is obtained, ranging from 181 to 277 cm^{-1} (see bottom part of Figure 4). Let us consider now the Ca isotopic shift in katoite (Figure 4 and Table 2, where only shifts larger than 1 cm^{-1} are reported). The "Ca band" in the full katoite spectrum ranges from 109 to 301 cm^{-1}; that is, it is larger by about 70 cm^{-1} on the low frequency side and 20 cm^{-1} on the high frequency side than the S_{Ca} band (note however the two modes at 431 and 656 cm^{-1}, that show some Ca contribution). If, somehow arbitrarily, we restrict the range to those modes with a Ca isotopic shift that is larger than 3.4 cm^{-1} (see frequencies below the dotted line in Figure 4), 15 modes are selected, which correspond to the 14 modes of the Γ_{Ca} representation plus an additional F_{1g} mode with a 3.5 cm^{-1} isotopic shift. The band of these 14 modes lies within a smaller range between 157.7 and 280 cm^{-1}, which, when compared with the S_{Ca} band, indicates that the main features of S_{Ca} are preserved in the full katoite spectrum and that coupling is limited, at least on the high frequency side.

TABLE 4: Observed and Calculated Raman-Active Modes of Katoite in the 160−800 cm^{-1} Range[a]

	calcd modes	obsd modes at $T = 298$ K		obsd modes at $T = 4$ K	
	ν	ν	$\Delta\nu$	ν	$\Delta\nu$
F_{2g}	163.4	163	−0.4		
F_{2g}	179.2			170	−9.2
F_{2g}	227.6	231	3.4	222	−5.6
E_g	250.4			250	−0.4
E_g	332.8	327	−5.8	334	1.2
F_{2g}	356.8	331	−25.8		
F_{2g}	373.5	366	−7.5		
F_{2g}	396.5	388	−8.5	398	1.5
A_g	503.8			486	−17.8
F_{2g}	540.8	535	−5.8	549	8.2
A_g	559.4	534	−25.4		
E_g	698.2			707	8.8
F_{2g}	757.0			756	−1.0
F_{2g}	782.1	780	−2.1		
F_{2g}	798.1			798	−0.1
$\overline{\lvert\Delta\rvert}$			9.4		5.4
Δ			−8.7		−2.3
Δ_{min}			−25.8		−17.8
Δ_{max}			3.4		8.8

[a] $\Delta\nu$ (cm^{-1}) is the difference between the present calculated data and the observed modes of ref 38, that are also used for the calculation of the statistical indices at the bottom of the table (see Table 1 for definitons).

Table 3 shows that the translation frequency of a single octahedron ($S_{Al(OH)_6}$), when the rest of the unit cell (including Ca cations) is frozen, can be as low as 164 cm^{-1}, and the rotation frequency is only about 40 cm^{-1} higher. When the other octahedra are allowed to vibrate in phase or out of phase, the translation and rotation frequencies can increase or decrease by a relatively large amount, particularly when a cooperative contribution from the Ca cations is also present, as is the case for most of the modes with frequencies between 300 and 100 cm^{-1}, as discussed above. Non-negligible contributions from the H rotations are also observed in a few cases (see last column in Table 2). The system presents 10 modes (F_{2u}, F_{1u}, B_u, F_{2g}) with frequencies in the range 60−100 cm^{-1}; they are essentially combinations of translation and rotation modes of the octahedra, coupled to H rotations and small movements of the Ca cations, as shown by animations.[41]

D. Comparison with Experimental IR and RAMAN Data. Besides the chemical work of Rossman,[4] very recently, IR and Raman measurements have been carried out by Kolesov and Geiger on synthetic hydrogrossular at a low temperature as well as at room temperature.[38] In regard to IR data, only two peaks due to the "lattice modes" are reported in that work; these peaks are not classified by symmetry, so that the comparison with computed data is impossible. Experimental Raman peaks, on the contrary, are more abundant and symmetry classified. Table 4 compares the two sets measured at $T = 298$ K and $T = 4$ K with the ab initio ones described above. The computed harmonic frequencies have been assigned to each experimental value according to symmetry coherence. However, the experimental symmetry assigment has only been possible for the spectra recorded at $T = 298$ K, so some uncertainty remains for the

association between the computed and measured values at low temperature. In general, the agreement is striking: the average error, $\overline{|\Delta|}$, is about 6 cm^{-1} (4 K) and 10 cm^{-1} (298 K) for the frequencies in the 160−800 cm^{-1} range.

As far as the OH strectching modes are concerned, the comparison is more delicate, due to the anharmonic correction. In section A, the $\omega_e x_e$ value related to the free decoupled OH stretching has been computed to be 86 cm^{-1}. If this value is also used to correct all of the active harmonic OH modes, the Raman and IR frequencies span the 3672−3689 and 3672−3686 cm^{-1} ranges, respectively, with a spread of ∼17 cm^{-1}. Comparison with experiment (at both low and high temperatures) shows for the Raman and IR spectra ranges at 3648−3699 and 3655−3701 cm^{-1}, respectively, with a spread of about ∼50 cm^{-1}, that is, 2−3 times larger than the calculated one. Considering on one hand the various approximations introduced to estimate anharmonicity and on the other hand the many assumptions implicit in the best-fit procedure adopted to interpret the experimental spectra in the OH region, the agreement can be considered very satisfactory.

IV. Conclusions

In the present paper, the full vibrational spectrum at the Γ point of katoite has been calculated at the ab initio quantum mechanical level, by using an all-electron Gaussian basis set and B3LYP. The full set of modes has been characterized by using several tools. It turns out that hydrogen modes are mostly "pure" modes and that stretching, bending, and rotation modes arise in different regions of the spectrum. At low frequencies, mixing of modes is larger. It mainly involves nearly rigid translations and rotations of the $Al(OH)_6$ octahedra, translations of the Ca cations, and H rotations, to give frequencies that can be as low as 60 cm^{-1}.

The present paper, that to our knowledge is the first successful attempt in this direction, shows that computing and fully characterizing the vibrational spectrum of large unit cell systems is now possible. Calculated vibration frequencies are expected to be as accurate as those that have been demonstrated in a recent application to pyrope,[34] for which both high quality IR and Raman experimental data were available.

Acknowledgment. CINECA supercomputing center is acknowledged for allowance of computer time. R.D. acknowledges Italian MURST for financial support (Cofin04 Project 25982_002 coordinated by R. Resta). F.J.T. acknowledges Regione Piemonte for his Ph.D. grant (Ab-initio simulation of the hydrogen storage process in microporous materials).

References and Notes

(1) Griggs, D. T.; Blacic, J. D. *Science* **1965**, *147*, 292.
(2) Wilkins, R. W. T.; Sabine, W. *Am. Mineral.* **1973**, *58*, 508.
(3) Beran, A.; Putnis, A. *Phys. Chem. Miner.* **1983**, *9*, 57.
(4) Rossman, G. R.; Aines, R. D. *Am. Mineral.* **1991**, *76*, 1153−1164.
(5) Nobes, R. H.; Akhmatskaya, E. V.; Milman, V.; White, J. A.; Winkler, B.; Pickard, C. J. *Am. Mineral.* **2000**, *85*, 1706−1715.
(6) Bell, D.; Rossman, G. *Science* **1992**, *255*, 1391.
(7) Passaglia, E.; Rinaldi, R. *Bull. Mineral.* **1984**, *107*, 605.
(8) Sacerdoti, M.; Passaglia, E. *Bull. Mineral.* **1985**, *108*, 1.
(9) Pascale, F.; Ugliengo, P.; Civalleri, B.; Orlando, R.; D'Arco, P.; Dovesi, R. *J. Chem. Phys.* **2004**, *121*, 1005−1013.
(10) Lager, G.; Dreele, R. V. *Am. Mineral.* **1996**, *81*, 1097−1104.
(11) Lager, G.; Armbruster, T.; Faber, J. *Am. Mineral.* **1987**, *72*, 756−765.
(12) Lager, G. A.; Ambruster, T.; Rotella, F. J.; Rossman, G. R. *Am. Mineral.* **1989**, *74*, 840.
(13) Schoenitz, M.; Navrotsky, A. *Am. Mineral.* **1999**, *84*, 389−391.
(14) Robie, R. A.; Hemingway, B. S.; Fisher, J. R. *Thermodynamic properties of minerals and related substances at 298.15 K and 1 bar (10^5 Pa) pressure and at higher temperatures*; U.S. Geol. Surv. Bull. 1452; United States Government Printing Office: Washington, D.C., 1978.
(15) Pascale, F.; Zicovich-Wilson, C. M.; Gejo, F. L.; Civalleri, B.; Orlando, R.; Dovesi, R. *J. Comput. Chem.* **2004**, *25*, 888.
(16) Zicovich-Wilson, C. M.; Pascale, F.; Roetti, C.; Orlando, V. R. S. R.; Dovesi, R. *J. Comput. Chem.* **2004**, *25*, 1873−1881.
(17) Tosoni, S.; Pascale, F.; Ugliengo, P.; Orlando, R.; Saunders: V. R.; Dovesi, R. *Mol. Phys.* **2005**, *103*, 2549−2558.
(18) Ugliengo, P.; Pascale, F.; Mérawa, M.; Labéguerie, P.; Tosoni, S.; Dovesi, R. *J. Phys. Chem. B* **2004**, *108*, 13632−13637.
(19) Pascale, F.; Tosoni, S.; Zicovich-Wilson, C. M.; Ugliengo, P.; Orlando, R.; Dovesi, R. *Chem. Phys. Lett.* **2004**, *396*, 308−315.
(20) Lager, G. A.; Downs, R. T.; Origlieri, M.; Garoutte, R. *Am. Mineral.* **2002**, *87*, 642.
(21) Olijnyk, H.; Paris, E.; Geiger, C. A.; Lager, G. A. *J. Geophys. Res.* **1991**, *96 B9*, 14313.
(22) Neill, O.; Bass, J. D.; Rossman, G. R.; Geiger, C. A.; Langer, K. *Phys. Chem. Miner.* **1991**, *17*, 617.
(23) Isaak, D. G.; Graham, E. K. *J. Geophys. Res.* **1976**, *81*, 2483.
(24) Saunders, V. R.; Dovesi, R.; Roetti, C.; Causà, M.; Harrison, N. M.; Orlando, R.; Zicovich-Wilson, C. M. *Crystal-98 user's manual*; Università di Torino: Torino, Italy, 1999.
(25) www.crystal.unito.it/Basis_Sets/ptable.html (accessed January 10, 2005).
(26) Becke, A. D. *J. Chem. Phys.* **1993**, *98*, 5648.
(27) Koch, W.; Holthausen, M. C. *A Chemist's Guide to Density Functional Theory*; Wiley-VCH Verlag GmbH: Weinheim, Germany, 2000.
(28) Prencipe, M.; Pascale, F.; Zicovich-Wilson, C. M.; Saunders: V. R.; Orlando, R.; Dovesi, R. *Phys. Chem. Miner.* **2004**, *31*, 559−564.
(29) Doll, K.; Harrison, N. M.; Saunders, V. R. *Int. J. Quantum Chem.* **2001**, *82*, 1.
(30) Doll, K. *Comput. Phys. Commun.* **2001**, *137*, 74.
(31) Orlando, R. Unpublished data.
(32) Civalleri, B.; D'Arco, P.; Orlando, R.; Saunders: V. R.; Dovesi, R. *Chem. Phys. Lett.* **2001**, *348*, 131.
(33) Schlegel, H. B. *J. Comput. Chem.* **1982**, *3*, 214.
(34) Pascale, F.; Zicovich-Wilson, C. M.; Orlando, R.; Roetti, C.; Ugliengo, P.; Dovesi, R. *J. Phys. Chem. B* **2005**, *109*, 6146−6152.
(35) Ugliengo, P. *Anharm—a program to solve the one-dimensional nuclear schroedinger equation*; Unpublished, **1978**.
(36) Ugliengo, P.; Viterbo, D.; Chiari, G. Moldraw Program, www.moldraw.unito.it (accessed June 5, 2005).
(37) Ugliengo, P.; Viterbo, D.; Chiari, G. *Z. Kristallogr.* **1993**, *207*, 9.
(38) Kolesov, B.; Geiger, C. *Am. Mineral.* **2005**, *90*, 1335−1341.
(39) Kolesov, B.; Geiger, C. *Phys. Chem. Miner.* **1998**, *25*, 142−151.
(40) Hofmeister, A.; Chopelas, A. *Phys. Chem. Miner.* **1991**, *17*, 503−526.
(41) Animation of katoite normal vibration modes. www.crystal.unito.it/supplement/Frequencies/vibrational_modes.html (accessed June 25, 2005).